ELSEVIER

Journal of Photochemistry and Photobiology
A: Chemistry 85 (1995) 173–178

Journal of
PHOTOCHEMISTRY
AND
PHOTOBIOLOGY
A:CHEMISTRY

Activation energies in semiconductor photocatalysis for water purification: the 4-chlorophenol–TiO_2–O_2 photosystem

Andrew Mills, Richard Davies

Department of Chemistry, University College of Swansea, Singleton Park, Swansea, SA2 8PP, UK

Received 25 April 1994; accepted May 19 1994

Abstract

The variation in the activation energy for the initial stage of photomineralization of 4-chlorophenol (4-CP), sensitized by Degussa P25 TiO_2, was investigated as a function of P_{O_2} and [4-CP]. A model was developed based on the incorporation of Arrhenius-type functions in a general rate equation for the initial stage of photomineralization. Values of the essential constants in the model were derived from a few simple experiments. Positive, negative and zero apparent activation energies were predicted using the model, and verified experimentally, under moderate reaction conditions. The general applicability of the model is briefly discussed.

Keywords: Activation energies; Semiconductor photocatalysis

1. Introduction

Semiconductor photocatalysts, such as TiO_2 and ZnO, can mediate the mineralization of a wide range of organics by oxygen, i.e.

$$\text{organic} + O_2 \xrightarrow[\text{ultra-band gap light}]{\text{semiconductor}} CO_2 + H_2O + \text{mineral acids} \quad (1)$$

This process has real potential as an alternative method for the purification of water and, as a result, has been the subject of extensive investigation [1]. The most popular semiconductor used for this work is TiO_2 due to its low cost, chemical and biochemical inertness and high photocatalytic activity (Degussa P25 TiO_2 is particularly photoactive).

In reaction (1), an important operational parameter is the temperature, and therefore in many of the studies of reaction (1), using different organic pollutants, the effect of temperature on the initial rate of disappearance of the organic species has been investigated [2–11]. If the initial rate of reaction (1) depends simply on the rate of generation of electron–hole pairs, the activation energy E_a will be zero. However, most researchers have reported a positive activation energy for reaction (1) [2–8], although some have reported zero or negative activation energies [9–11], as indicated by the list of reported activation energies for the photomineralization of different compounds sensitized by Degussa P25 TiO_2 given in Table 1 [2–11]. It should be noted that, in the studies given in Table 1 and in this work, the activation energy E_a for reaction (1) refers to the activation energy associated with the initial rate of disappearance of the organic. Clearly, if, for a particular example of reaction (1), one or more substantial stable reaction intermediates are generated before any CO_2 is evolved, the measured activation energy for CO_2 evolution may well be different from E_a.

Table 1
Previously reported activation energies for reaction (1), sensitized by Degussa P25 TiO_2

Organic	E_a (kJ mol^{-1})	Reference
Formic acid	17	[2]
Oxalic acid	13	[3]
Phenol	10	[4]
4-Chlorophenol	16	[5]
4-Chlorophenol	5.5	[6]
Salicylic acid	11[a]	[7]
Salicylic acid	4.6	[8]
1,1,1-Trichloroethane, tetrachloroethane, chlorobenzene	0	[9]
Reactive Black 5	0	[10]
Chloroform	−ve	[11]

[a]Carried out in a flow reactor (all others used batch reactors).

SSDI 1010-6030(94)03890-7

From the data given in Table 1, it can be seen that E_a for reaction (1) sensitized by TiO_2 is different for different pollutants. However, surprisingly, E_a may be different for the same organic pollutant (e.g. 4-chlorophenol or salicylic acid). In most cases, such differences can be attributed to the combination of different reaction conditions during the measurements and the ubiquitous experimental error. It is probable that the activation energy for reaction (1) will be a function of the semiconductor type and nature (e.g. if the semiconductor is TiO_2 whether it is anatase or rutile), the photoreactor type and operational conditions (e.g. flow or batch photoreactor, stirred or unstirred, flow rate) and the nature of the organic compound (ease of oxidation). In addition, on inspection of the commonly observed rate law for reaction (1) (see below), E_a is likely to be a function of the concentration of the organic pollutant under test and the partial pressure of O_2 (P_{O_2}) used to saturate the test solution. As a result, useful comparisons are hard to make between the activation energies for reaction (1) reported by different research groups.

In an attempt to define a standard test system for semiconductor-photosensitized water purification, we have recently reported the results of a detailed study of the kinetics and reaction intermediates associated with the photomineralization of 4-chlorophenol (4-CP), sensitized by Degussa P25 TiO_2 [5,12], i.e.

$$ClC_6H_4OH + 6\tfrac{1}{2}O_2 \xrightarrow[TiO_2]{h\nu \geq 3.2\ eV} 6CO_2 + 2H_2O + HCl \quad (2)$$

As part of our effort to characterize this reaction further, we have investigated the variation in the apparent activation energy for the initial photodestruction of 4-CP, sensitized by Degussa P25 TiO_2, as a function of [4-CP] and P_{O_2}.

2. Experimental details

2.1. Materials

The titanium dioxide used throughout this work was Degussa P25 TiO_2. 4-CP (99%) was obtained from Aldrich Chemicals and was used as received. The perchloric acid solution used to adjust the pH of the reaction solution to its usual value of pH 2 was BDH AnalaR grade perchloric acid (60%–62% by weight). The methanol used for high performance liquid chromatography (HPLC) analysis was also BDH AnalaR grade. The gases used to alter the P_{O_2} value of the reaction solution were nitrogen (oxygen free) and oxygen (both obtained from BOC). In this work, all the water used to make up the solutions was deionized and doubly distilled.

2.2. The photochemical reactor and reaction vessel

The photochemical reactor comprised two half-cylinders, each of which contained six 8 W Coast-Wave Blacklight UVA lamps set against an aluminium reflector. The number of lamps used in most experiments was 12, but six or two lamps were used when the initial [4-CP] value was low. The reaction vessel was a Pyrex Dreschel bottle (125 cm^3) fitted with a glass stopper, a rubber septum and a thermostatically controlled outer water jacket (temperatures were fixed within the range 20–60 °C). The photochemical reactor and reaction vessel have been described in detail elsewhere [12]. The P_{O_2} value of the gas used to saturate the reaction solution was adjusted to the desired value using a Signal series 850 gas blender.

In a typical experiment, 50 mg of TiO_2 and 100 μl of perchloric acid were added to 100 ml of a 4-CP solution (10^{-2}–10^{-5} mol dm^{-3}). These reaction solutions were purged, with a defined mixture of nitrogen and oxygen, and stirred for 20 min prior to and during irradiation.

2.3. Analyses

Quantitative analysis of 4-CP within the reaction solution was performed by HPLC (LDC/Milton Roy) using a Constametric 3500 solvent delivery system, a guard column (to remove particulate matter), an analytical column (length, 25 cm; inside diameter, 4.6 mm) packed with Spherisorb ODS, a variable wavelength detector (LDC SM 4000) set at 280 nm and an LDC CI-4100 Integrator chart recorder. The solvent was a methanol–water mixture (60 : 40) pumped at 1 cm^3 min^{-1}, which eluted all the major components from the column within 10 min. All samples were filtered using a 0.2 μm cellulose filter, prior to analysis by HPLC, to remove the TiO_2 particles.

3. A kinetic model

From the results of numerous kinetic studies of reaction (1), it has been established [1] that the initial rate of disappearance R_i of the organic species is usually described by an expression of the following form

$$R_i = \gamma I^{\theta} \frac{K_{O_2} P_{O_2}}{(1 + K_{O_2} P_{O_2})} \frac{K_S[S]}{(1 + K_S[S])} \quad (3)$$

where γ is a proportionality constant, I is the intensity of incident ultra-band gap light and θ is a power term which is equal to 0.5 or unity at high or low light intensities respectively.

Originally K_{O_2} and K_S were assumed to be the Langmuir adsorption constants for O_2 and S on the surface of the semiconductor. However, this idea has lost cred-

ibility following the work of Cunningham et al. [13] who, for a number of different pollutants, showed that the value of the Langmuir adsorption constant measured in the dark was much lower than the value of K_S determined via a photocatalytic kinetic study. Turchi and Ollis [14] have proposed four possible different mechanisms for reaction (1) involving hydroxyl radical attack, all of which yield a rate equation of the form of Eq. (3). In each scheme the fundamental interpretation of the constant K_S is different and none is simply equivalent to the dark Langmuir adsorption constant.

Whatever the actual mechanism(s) of semiconductor photocatalysis, given that the initial kinetics of reaction (1) are usually described by an expression of the form of Eq. (3), it seems reasonable to assume, initially at least, that each of the three terms (γ, K_{O_2} and K_S) is a function of temperature and can be described by the following Arrhenius-type expressions

$$\gamma = \bar{\gamma} \exp(-E_{a1}/RT) \quad (4)$$

$$K_{O_2} = \bar{K}_{O_2} \exp(-E_{a2}/RT) \quad (5)$$

$$K_S = \bar{K}_S \exp(-E_{a3}/RT) \quad (6)$$

where $\bar{\gamma}$, $\bar{K}_{O_2}$ and $\bar{K}_S$ are the values of γ, K_{O_2} and K_S at infinite temperature. The combination of Eq. (3) with Eqs. (4)–(6) generates the following expression

$$R_i = \bar{\gamma} \exp(-E_{a1}/RT) I^{\theta} \frac{\bar{K}_{O_2} \exp(-E_{a2}/RT) P_{O_2}}{[1 + \bar{K}_{O_2} \exp(-E_{a2}/RT) P_{O_2}]} \times \frac{\bar{K}_S \exp(-E_{a3}/RT)[S]}{[1 + \bar{K}_S \exp(-E_{a3}/RT)[S]]} \quad (7)$$

which we shall assume provides a complete expression for the variation of R_i as a function of temperature.

In order to use Eq. (7) to predict the variation of R_i as a function of temperature, for any combination of P_{O_2} and [S], the values of the following constants need to be determined experimentally: $\bar{\gamma}$, E_{a1}, $\bar{K}_{O_2}$, E_{a2}, $\bar{K}_S$ and E_{a3}. This objective may be achieved via a series of kinetic experiments carried out under the following three very different sets of experimental conditions.

(1) Under conditions of high P_{O_2} and high [S], the second and third terms in Eq. (7) will make little or no contribution to the value of R_i and, therefore, E_{a1} can be determined from the gradient of an Arrhenius plot of $\ln(R_i)$ vs. $1/T$. Once the value of E_{a1} has been obtained, the value of $\bar{\gamma}$ can then be calculated from the value of R_i at any particular temperature (e.g. 25 °C) measured under the same experimental conditions.

(2) After having performed the experiments described in (1), the contribution of the first term in Eq. (7) to the overall value of R_i as a function of temperature will be known and can be allowed for. Under conditions of high [S] and low P_{O_2}, the third term in Eq. (7) will make little or no contribution to the value of R_i at any temperature, and the second term will approximate to $\bar{K}_{O_2} \exp(-E_{a2}/RT) P_{O_2}$. As a result, under these conditions, E_{a2} can be determined from the gradient of the Arrhenius plot of $\ln(R_i)$ vs. $1/T$. Once the value of E_{a2} has been determined, the value of $\bar{K}_{O_2}$ can then be calculated via Eq. (5) from a value determined for K_{O_2} at any particular temperature (e.g. 25 °C) measured under conditions of high [S]; K_{O_2} at any temperature can be determined by measuring R_i as a function of P_{O_2}, since K_{O_2} is equal to the ratio of the values of the intercept to the gradient associated with a plot of the data in the form $1/R_i$ vs. $1/P_{O_2}$.

(3) Under conditions of high P_{O_2} and low [S], the second term in Eq. (7) will make little or no contribution to the value of R_i at any temperature, and the third term will approximate to $\bar{K}_S \exp(-E_{a3}/RT)[S]$. As a result, under these conditions, E_{a3} can be determined from the gradient of the Arrhenius plot of $\ln(R_i)$ vs. $1/T$. Once the value of E_{a3} has been determined, the value of $\bar{K}_S$ can then be calculated via Eq. (6) from a value determined for K_S at any particular temperature (e.g. 25 °C) measured under conditions of high P_{O_2}; K_S at any temperature can be determined by measuring R_i as a function of P_{O_2}, since K_S is equal to the ratio of the values of the intercept to the gradient associated with a plot of the data in the form $1/R_i$ vs. $1/[S]$.

4. Results and discussion

The initial kinetics of photodestruction of 4-CP, sensitized by Degussa P25 TiO_2, i.e. reaction (2), were studied as a function of temperature under the three different reaction condition regimes outlined in the previous section. All other reaction conditions were as described in Section 2.

4.1. Kinetics at high P_{O_2} and high [4-CP]

The initial rate of reaction (2) was found to be temperature independent over the range 20–60 °C under conditions of high P_{O_2} (1 atm) and high [4-CP] (0.01 mol dm^{-3}). From the results of this work, the value for E_{a1} was taken as 0 kJ mol^{-1} and $\bar{\gamma} = 4.0 \times 10^{-5}$ mol dm^{-3} min^{-1}.

4.2. Kinetics at high [4-CP] and low P_{O_2}

R_i was determined as a function of temperature, spanning the range 20–50 °C, under conditions of high [4-CP] (5×10^{-3} mol dm^{-3}) and low P_{O_2} (0.02 atm). The results of this work, together with an Arrhenius plot of the data, are illustrated in Fig. 1. From the gradient of the Arrhenius plot a value for E_{a2} of -15 kJ mol^{-1} was calculated. R_i was then measured as a function of P_{O_2} over the range 0–1 atm at 25 °C, with

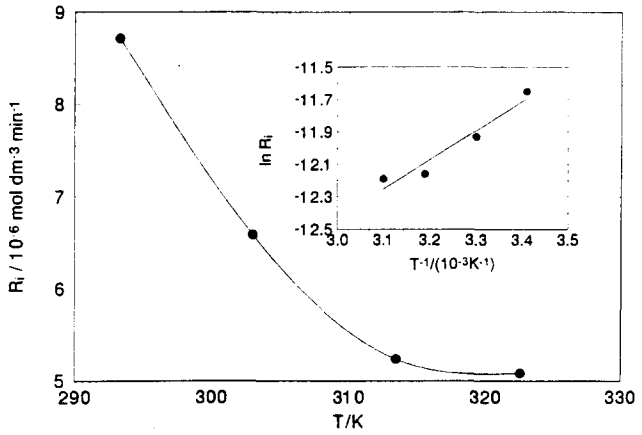

Fig. 1. Plot of the initial rate of destruction of 4-CP (R_i) vs. reaction temperature (spanning the range 20–50 °C); the other reaction conditions were as follows: reaction solution volume, 100 cm^3; $[TiO_2]=0.5$ mg cm^{-3}; $P_{O_2}=0.02$ atm; $[4\text{-CP}]=5\times10^{-3}$ mol dm^{-3}; pH 2. The inset shows the subsequent Arrhenius plot of the data, a least-squares analysis of which reveals the following: number of points (n)=4; gradient (m)=$(1.8\pm0.3)\times10^3$ K; intercept (c)=-17.8 ± 1.1; correlation coefficient (r)=0.9672.

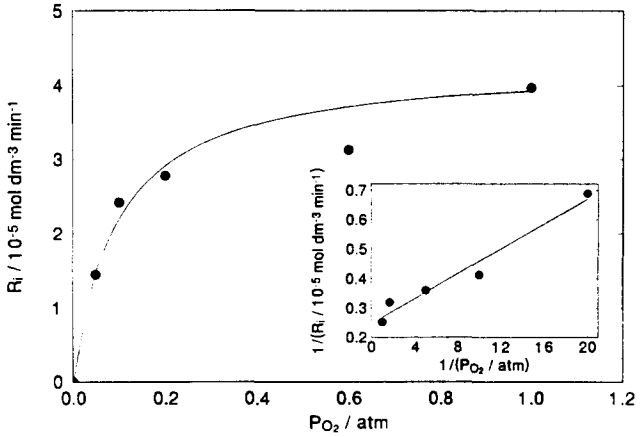

Fig. 2. Plot of R_i vs. P_{O_2} (spanning the range 0–1 atm) at 25 °C with all other reaction conditions as described for Fig. 1. The inset shows the subsequent double reciprocal plot of the data, a least-squares analysis of which reveals the following: $n=5$; $m=(2.2\pm0.3)\times10^3$ atm min dm^3 mol^{-1}; $c=(2.3\pm0.3)\times10^4$ min dm^3 mol^{-1}; $r=0.9752$.

$[4\text{-CP}]=5\times10^{-3}$ mol dm^{-3}; the results of this work, together with a double reciprocal plot of the data, are illustrated in Fig. 2. From the ratio of the values of the intercept and gradient of the line of best fit to the data, a value of $K_{O_2}=10.5$ atm^{-1} at 25 °C was calculated and used to obtain a value for $\bar{K}_{O_2}$ of 0.025 atm^{-1} ($\bar{K}_{O_2}=K_{O_2}/\exp(-E_{a2}/RT)$).

4.3. Kinetics at high P_{O_2} and low [4-CP]

R_i was determined as a function of temperature, spanning the range 20–60 °C, under conditions of high P_{O_2} (1 atm) and low [4-CP] (10^{-5} mol dm^{-3}). The results of this work, together with an Arrhenius plot of the data, are illustrated in Fig. 3. From the gradient of the Arrhenius plot, a value for E_{a2} of 6.4 kJ mol^{-1} was calculated. R_i was then measured as a function of [4-CP] over the range 0–10^{-3} mol dm^{-3} at 25 °C, with $P_{O_2}=1$ atm, and the results of this work, together with a double reciprocal plot of the data, are illustrated in Fig. 4. From the ratio of the values of the intercept and gradient of the line of best fit to the data, a value of $K_S=3.4\times10^3$ dm^3 mol^{-1} at 25 °C was calculated and used to obtain a value for $\bar{K}_S$ of 4.5×10^4 dm^3 mol^{-1} ($\bar{K}_S=K_S/\exp(-E_{a3}/RT)$).

4.4. E_a as a function of P_{O_2} and [4-CP]

From the results of the work described in Sections 4.1–4.3, values for the constants $\bar{\gamma}$, E_{a1}, $\bar{K}_{O_2}$, E_{a2}, $\bar{K}_S$ and E_{a3} were determined and are collected in Table

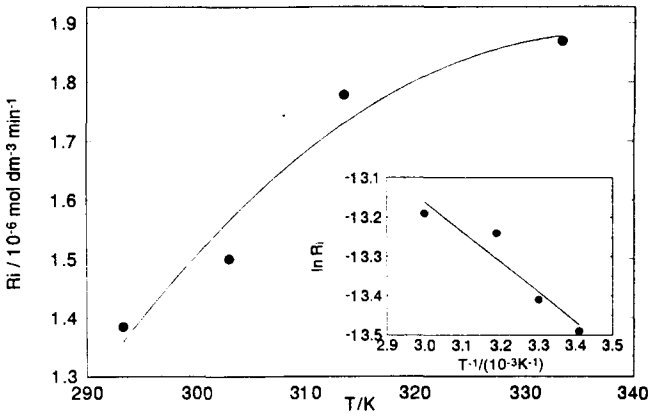

Fig. 3. Plot of R_i vs. reaction temperature (spanning the range 20–60 °C); the other reaction conditions were as follows: reaction solution volume, 100 cm^3; $[TiO_2]=0.5$ mg cm^{-3}; $P_{O_2}=1.0$ atm; $[4\text{-CP}]=10^{-5}$ mol dm^{-3}; pH 2. The inset shows the subsequent Arrhenius plot of the data, a least-squares analysis of which reveals the following: $n=4$; $m=-(7.7\pm1.8)\times10^2$ K; $c=-10.9\pm0.6$; $r=0.9497$.

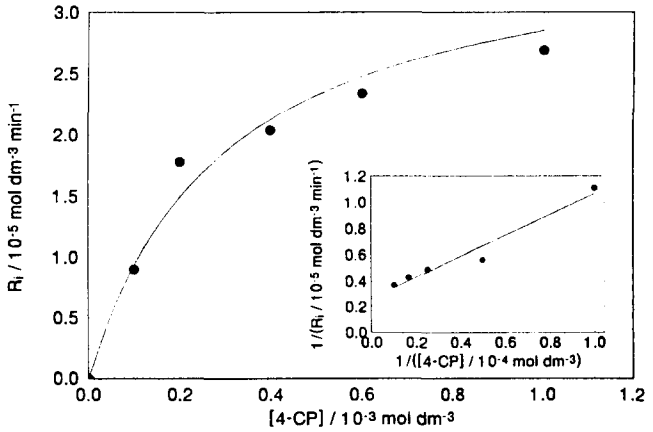

Fig. 4. Plot of R_i vs. [4-CP] (spanning the range 0–10^{-3} mol dm^{-3}) at 25 °C with all other reaction conditions as described for Fig. 3. The inset shows the subsequent double reciprocal plot of the data, a least-squares analysis of which reveals the following: $n=5$; $m=8.0\pm1.0$ min; $c=(2.7\pm0.5)\times10^4$ min dm^3 mol^{-1}; $r=0.9791$.

2. Using these values, in combination with Eq. (7), it is possible to calculate R_i for reaction (2) for any given combination of temperature, P_{O_2} and [4-CP].

In practice, most researchers determine the apparent activation energy for reaction (1) by simply measuring R_i as a function of temperature under "typical" conditions, i.e. for a particular favoured set of values of [S] and P_{O_2}; the apparent activation energy is readily extracted from an Arrhenius plot of the data arising from such a study. It is tempting to assume that this apparent activation energy applies for all combinations of P_{O_2} and [S]. However, it is clear from our work on reaction (2), and the results in Table 2, that this assumption is unreliable.

In order to illustrate this point more clearly, the constants in Table 2 were used in combination with Eq. (7) to generate a series of values for R_i as a function of temperature, over the range 20–60 °C, for an arbitrarily chosen set pair of values for P_{O_2} and [4-CP]. From a subsequent Arrhenius plot of the data an "apparent" activation energy was calculated for the set pair of values of P_{O_2} and [4-CP] chosen. This exercise was then repeated many times, using different set values for P_{O_2} and [4-CP], spanning the range 10^{-4}–1 atm and 10^{-7}–0.1 mol dm^{-3} respectively, in order to generate a series of apparent activation energy values for different set pair values of P_{O_2} and [4-CP]. The results of this work are illustrated in Figs. 5(a) and 5(b) from two different perspectives, together with the apparent activation energies for reaction (2) determined experimentally using the P_{O_2} and [4-CP] values given in Table 3. The agreement between the model-generated apparent activation energies and those determined experimentally in this work (points A–F) is quite good. The model-predicted and experimentally determined values (especially points B, C and D) illustrate that, not only is the apparent activation energy for reaction (2) a function of P_{O_2} and [4-CP], but it can also be positive, zero or negative under moderate reaction conditions.

Also shown in Fig. 5, as data point G, is the activation energy for reaction (2) reported by Al-Sayyed et al. [6] (see Table 1), which appears to fit in quite well with the model-predicted variation in E_a for reaction (2) as a function of P_{O_2} and [4-CP]. In contrast, the activation energy value of 16 kJ mol^{-1}, previously reported by our group for reaction (2) [5] (see Table 1), does not fit the model-predicted variation in E_a. This discrepancy arises because the activation energy value of 16 kJ mol^{-1} was determined from a study of the rate of generation of CO_2 due to reaction (2) as a function of temperature and, therefore, is a measure of E_a for the overall mineralization reaction [5]. Thus the latter activation energy cannot be compared simply with the activation energies reported in the current

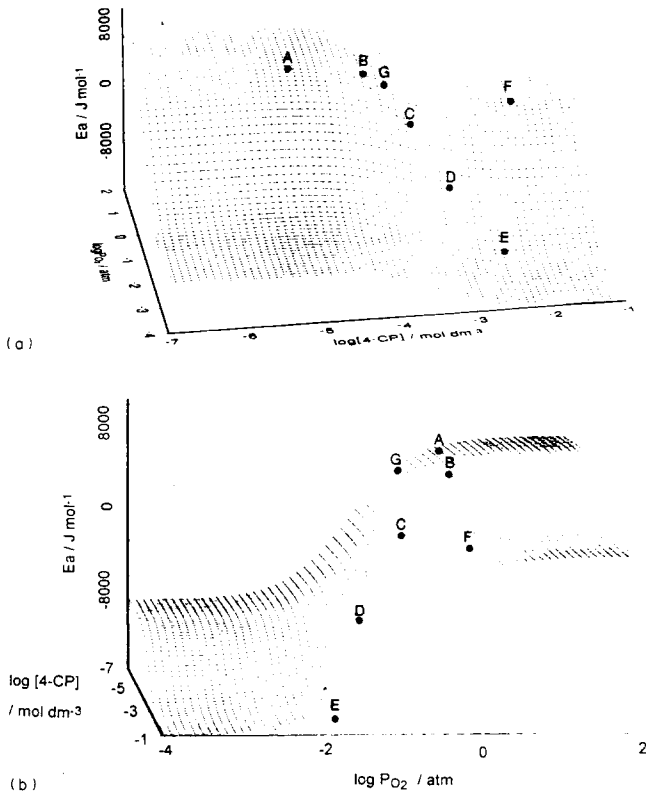

Fig. 5. Plot of the apparent activation energy from two viewpoints for reaction (2), calculated using Eq. (7) of the kinetic model and the experimentally determined constants listed in Table 2. The key experimental parameters associated with data points A–G are given in Table 3.

Table 2
Experimentally determined values for the constants in Eq. (7)

Constant	Value
$\bar{\gamma}$ (mol dm^{-3} min^{-1})	4.0×10^{-5}
E_{a1} (kJ mol^{-1})	0
K_{O2} (atm^{-1})	0.025
E_{a2} (kJ mol^{-1})	−15
K_S (dm^3 mol^{-1})	4.5×10^4
E_{a3} (kJ mol^{-1})	6.4

Table 3
Experimental conditions used to obtain the data points A–G in Fig. 5

Data point	[4-CP] (mol dm^{-3})	P_{O2} (atm)	Number of lamps	Apparent activation energy (kJ mol^{-1})
A	10^{-5}	1.00	2	6.4 ± 1.5
B	10^{-4}	1.00	6	5.0 ± 1.2
C	3.5×10^{-4}	0.20	6 or 12	0
D	10^{-3}	0.05	12	−7.1 ± 0.6
E	5×10^{-3}	0.02	12	−15 ± 2.8
F	10^{-2}	1.00	12	0
G[a]	1.55×10^{-4}	0.2	–	5.5

[a]Data from Ref. [6].

study (see Fig. 5) which refer to the initial rate of disappearance of 4-CP, rather than the overall rate of photomineralization. That the two activation energies are not the same is hardly surprising given that in the photomineralization of 4-CP, sensitized by Degussa P25 TiO_2, a considerable fraction of the 4-CP is initially converted to relatively stable hydroxylated intermediates, such as 4-chlorocatechol and hydroquinone, before being mineralized [12].

5. Conclusions

The variation in the activation energy for the initial stage of photomineralization of 4-CP, sensitized by Degussa P25 TiO_2, is a complex function of P_{O_2} and [4-CP] which can be successfully modelled using Arrhenius-type functions in a general rate equation and essential constants derived from a few simple experiments. Positive, negative and zero apparent activation energies can be obtained experimentally under moderate reaction conditions, and agree with those predicted using the model. It is likely that the model can be applied to many other photomineralization studies. Thus, in the future, an activation energy study for a different photomineralization process may benefit from the results of a few, carefully constructed, simple experiments and application of the kinetic model, rather than the usual single activation energy experiment carried out under "typical" reaction conditions involving one set of values of P_{O_2} and [S].

Acknowledgement

We thank the Science and Engineering Research Council (SERC) for support of this work via grant no. GR/H/25010.

References

[1] A. Mills, R.H. Davies and D. Worsley, *Chem. Soc. Rev.*, (1993) 417, and references cited therein.
[2] M. Bideau, B. Claudel and M. Otterbien, *J. Photochem. Photobiol, A: Chem., 14* (1980) 291.
[3] J.-M. Herrmann, M.-N. Mozzanega and P. Pichat, *J. Photochem. Photobiol. A: Chem., 22* (1983) 333.
[4] K. Okamoto, Y. Yamamoto, H. Tanaka, M. Tanaka and A. Itaya, *Bull. Chem. Soc. Jpn., 58* (1985) 2023.
[5] A. Mills and S. Morris, *J. Photochem. Photobiol. A: Chem., 71* (1993) 75.
[6] G. Al-Sayyed, J.-C. D'Oliveira and P. Pichat, *J. Photochem. Photobiol. A: Chem., 58* (1991) 99.
[7] R.W. Matthews, *J. Phys. Chem., 91* (1987) 3328.
[8] A. Mills, C. Holland, R.H. Davies and D. Worsley, *J. Photochem. Photobiol. A: Chem.*, accepted for publication.
[9] T.P.M. Koster, J.W. Assink, J.M. Slaager and C. van der Veen, in D.F. Ollis and H. Al-Ekabi (eds.), *Photocatalytic Purification and Treatment of Water and Air*, Elsevier, Amsterdam, 1993, p. 613.
[10] A. Mills and R. Davies, in D.F. Ollis and H. Al-Ekabi (eds.), *Photocatalytic Purification and Treatment of Water and Air*, Elsevier, Amsterdam, 1993, p. 595.
[11] D. Bahnemann, D. Bockelmann and R. Goslich, *Sol. Energy Mater., 24* (1991) 564.
[12] A. Mills, S. Morris and R. Davies, *J. Photochem. Photobiol. A: Chem., 70* (1993) 183.
[13] J. Cunningham, G. Al-Sayyed and S. Srijaranai, in G.R. Helz, R.G. Zepp and D.G. Crosby (eds.), *Aquatic and Surface Photochemistry*, Lewis Publishers, Boca Raton, 1994, pp. 317–348.
[14] C.S. Turchi and D.F. Ollis, *J. Catal., 122* (1990) 178.